CHAPTER 1

SCENE MODELING AND IMAGE MINING WITH A VISUAL GRAMMAR

Selim Aksoy, Carsten Tusk, Krzysztof Koperski, Giovanni Marchisio

Insightful Corporation
1700 Westlake Ave. N., Suite 500, Seattle, WA 98109, USA
E-mail: {saksoy,ctusk,krisk,giovanni}@insightful.com

Automatic content extraction, classification and content-based retrieval are highly desired goals in intelligent remote sensing databases. Pixel level processing has been the common choice for both academic and commercial systems. We extend the modeling of remotely sensed imagery to three levels: Pixel level, region level and scene level. Pixel level features are generated using unsupervised clustering of spectral values, texture features and ancillary data like digital elevation models. Region level features include shape information and statistics of pixel level feature values. Scene level features include statistics and spatial relationships of regions. This chapter describes our work on developing a probabilistic visual grammar to reduce the gap between low-level features and high-level user semantics, and to support complex query scenarios that consist of many regions with different feature characteristics. The visual grammar includes automatic identification of region prototypes and modeling of their spatial relationships. The system learns the prototype regions in an image collection using unsupervised clustering. Spatial relationships are represented by fuzzy membership functions. The system automatically selects significant relationships from training data and builds visual grammar models which can also be updated using user relevance feedback. A Bayesian framework is used to automatically classify scenes based on these models. We demonstrate our system with query scenarios that cannot be expressed by traditional region or scene level approaches but where the visual grammar provides accurate classifications and effective retrieval.

1. Introduction

Remotely sensed imagery has become an invaluable tool for scientists, governments, military, and the general public to understand the world and its surrounding environment. Automatic content extraction, classification and content-based retrieval are highly desired goals in intelligent remote sensing databases. Most of the current systems use spectral information or texture features as the input for statistical classifiers that are built using unsupervised or supervised algorithms. The most commonly used classifiers are the minimum distance classifier and the maximum likelihood classifier with a Gaussian density assumption. Spectral signatures and texture features do not always map conceptually similar patterns to nearby locations in the feature space and limit the success of minimum distance classifiers. Furthermore, these features do not always have Gaussian distributions so maximum likelihood classifiers with this assumption fail to model the data. Image retrieval systems also use spectral or texture features[2] to index images and then apply distance measures[3] in these feature spaces to find similarities. However, there is a large semantic gap between the low-level features and the high-level user expectations and search scenarios.

Pixel level processing has been the common choice for both academic and commercial land cover analysis systems where classifiers have been applied to pixel level measurements. Even though most of the proposed algorithms use pixel level information, remote sensing experts use spatial information to interpret the land cover. Hence, existing systems can only be partial tools for sophisticated analysis of remotely sensed data where a significant amount of expert involvement becomes inevitable. This motivated the research on developing algorithms for region-based analysis with examples including conceptual clustering,[38] region growing[9] and Markov random field models[34] for segmentation of natural scenes; hierarchical segmentation for image mining;[41] rule-based region classification for flood monitoring;[20] region growing for object level change detection;[13] boundary delineation of agricultural fields;[32] and task-specific region merging for road extraction and vegetation area identification.[42]

Traditional region or scene level image analysis algorithms assume that the regions or scenes consist of uniform pixel feature distributions. However, complex query scenarios and image scenes of interest usually contain many pixels and regions that have different feature characteristics. Furthermore, two scenes with similar regions can have very different interpretations if the regions have different spatial arrangements. Even when pixels and regions can be identified correctly, manual interpretation is necessary for studies like landing zone and troop movement planning in military applications and public health and ecological studies in civil applications. Example scenarios include studies on the effects of climate change and human intrusion into previously uninhabited tropical areas, and relationships between vegetation coverage, wetlands and habitats of animals carrying viruses that cause infectious diseases like malaria, West Nile fever, Ebola hemorrhagic fever and tuberculosis.[12,30] Remote sensing imagery with land cover maps and spatial analysis is used for identification of risk factors for locations to which infections are likely to spread. To assist developments in new remote sensing applications, we need a higher level visual grammar to automatically describe and process these scenarios.

Insightful Corporation's VisiMine system[17,18] supports interactive classification and retrieval of remotely sensed images by modeling them on pixel, region and scene levels. Pixel level characterization provides classification details for each pixel with regard to its spectral, textural and ancillary (e.g. DEM or other GIS layers) attributes. Following a segmentation process that computes an approximate polygon decomposition of each scene, region level features describe properties shared by groups of pixels. Scene level features describe statistical summaries of pixel and region level features, and the spatial relationships of the regions composing a scene. This hierarchical scene modeling bridges the gap between feature extraction and semantic interpretation. VisiMine also provides an interactive environment for training customized semantic labels from a fusion of visual attributes.

Overviews of different algorithms in VisiMine were presented in our recent papers.[26,25,23,24,19,17,16,18] This chapter describes our work on developing a probabilistic visual grammar[4] for scene level image mining. Our approach includes learning prototypes of primitive regions and their spatial relationships for higher-level content extraction, and automatic and supervised algorithms for using the visual grammar for content-based retrieval and classification.

Early work on spatial relationships of regions in image retrieval literature included the VisualSEEk project[37] where Smith and Chang used representative colors, centroid locations and minimum bounding rectangles to index regions, and computed similarities between region groups by matching them according to their colors, absolute and relative locations. Berretti *et al.*[5] used four quadrants of the Cartesian coordinate system to compute the directional relationship between a pixel and a region in terms of the number of pixels in the region that were located in each of the four quadrants around that particular pixel. Then, they extended this representation to compute the relationship between two regions using a measure of the number of pairs of pixels in these regions whose displacements fell within each of the four directional relationships. Centroids and minimum bounding rectangles are useful when regions have circular or rectangular shapes but regions in natural scenes often do not follow these assumptions.

Previous work on modeling of spatial relationships in remote sensing applications utilized the concept of spatial association rules. Spatial association rules[15,24] represent topological relationships between spatial objects, spatial orientation and ordering, and distance information. A spatial association rule is of the form $X \rightarrow Y(c\%)$, where X and Y are sets of spatial or non-spatial predicates and $c\%$ is the confidence of the rule. An example spatial association rule is *prevalent_endmember(x,concrete)* $\wedge$ *texture_class(x,*c_1*)* $\rightarrow$ *close_to(x,coastline) (60%)*. This rule states that 60% of regions where concrete is the prevalent endmember and that texture features belong to class c_1 are close to a coastline. Examples of spatial predicates include topological relations such as *intersect*, *overlap*, *disjoint*, spatial orientations such as *left_of* and *west_of*, and distance information such as *close_to* or *far_away.*

Similar work has also been done in the medical imaging area but it usually requires manual delineation of regions by experts. Shyu *et al.*[36] developed a content-based image retrieval system that used features locally computed from manually delineated regions. Neal *et al.*[28] developed topology, part-of and spatial association networks to symbolically model partitive and spatial adjacency relationships of anatomical entities. Tang *et al.*[39,40] divided images into small sub-windows, and trained neural network classifiers using color and Gabor texture features computed from these sub-windows and the labels assigned to them by experts. These classifiers were then used to assign labels to sub-windows in unknown images, and the labels were verified using a knowledge base of label spatial relationships that was created by experts. Petrakis and Faloutsos[29] used attributed relational graphs to represent features of objects and their relationships in magnetic resonance images. They assumed that the graphs were already known for each image in the database and concentrated on developing fast search algorithms. Chu *et al.*[7] described a knowledge-based semantic image model to represent image objects' characteristics. Graph models are powerful representations but are not usable due to the infeasibility of manual annotation in large databases. Different structures in remote sensing images have different sizes so fixed sized grids cannot capture all structures either.

Our work differs from other approaches in that recognition of regions and decomposition of scenes are done automatically, and training of classifiers requires only a small amount of supervision in terms of example images for classes of interest. The rest of the chapter is organized as follows. An overview of hierarchical scene modeling is given in Sec. 2. The concept of prototype regions is defined in Sec. 3. Spatial relationships of these prototype regions are described in Sec. 4. Algorithms for image retrieval and classification using the spatial relationship models are discussed in Secs. 5 and 6, respectively. Conclusions are given in Sec. 7.

2. Hierarchical Scene Modeling

In VisiMine, we extend the modeling of remotely sensed imagery to three levels: Pixel level, region level and scene level. Pixel level representations include land cover labels for individual pixels (e.g. water, soil, concrete, wetland, conifer, hardwood). Region level representations include shape information and labels for groups of pixels (e.g. city, residential area, forest, lake, tidal flat, field, desert). Scene level representations include interactions of different regions (e.g. forest near a water source, city surrounded by mountains, residential area close to a swamp). This hierarchical scene representation aims to bridge the gap between data and high-level semantic interpretation.

The analysis starts from raw data. Then, features are computed to build classification models for information fusion in terms of structural relationships. Finally, spatial relationships of these basic structures are computed for higher level modeling. Levels of the representation hierarchy are described below.

2.1. *Raw Data*

The lowest level in the hierarchy is the raw data. This includes multispectral data and ancillary data like Digital Elevation Models (DEM) or GIS layers. Examples are given in Figs. 1(a)–1(b).

2.2. *Features*

Feature extraction is used to achieve a higher level of information abstraction and summarization above raw data. To enable processing in pixel, region and scene levels, we use the following state-of-the-art feature extraction methods:

- Pixel level features:
  1. Statistics of multispectral values,
  2. Spectral unmixing for surface reflectance (spectral mixture analysis),[25]
  3. Gabor wavelet features for microtexture analysis,[22]
  4. Gray level co-occurrence matrix features for microtexture analysis,[10]
  5. Laws features for microtexture analysis,[21]
  6. Elevation, slope and aspect computed from DEM data,
  7. Unsupervised clustering of spectral or texture values.
- Region level features:
  1. Segmentation to find region boundaries (a Bayesian segmentation algorithm under development at Insightful, a hierarchical segmentation algorithm,[41] and a piecewise-polynomial multiscale energy-based region growing segmentation algorithm[14]),
  2. Shape information as area, perimeter, centroid, minimum bounding rectangle, orientation of the principal axis, moments, and roughness of boundaries,
  3. Statistical summaries (relative percentages) of pixel level features for each region.
- Scene level features:
  1. Statistical summaries of pixel and region level features for each scene,
  2. Spatial relationships of regions in each scene.

VisiMine provides a flexible tool where new feature extraction algorithms can be added when new data sources of interest are available. Examples for pixel level features are given in Figs. 1(c)–1(h). Example region segmentation results are given in Figs. 2(a) and 2(c).

2.3. *Structural Relationships*

We use a Bayesian label training algorithm with naive Bayes models[35] to perform fusion of multispectral data, DEM data and the extracted features. The Bayesian framework provides a probabilistic link between low-level image feature attributes and high-level user defined semantic structure labels. The naive Bayes model uses the conditional independence assumption and allows the training of class-conditional probabilities for each attribute. Training for a particular semantic label is done using user labeling of pixels or regions as positive or negative examples for that particular label under training. Then, the probability of a pixel or region belonging to that

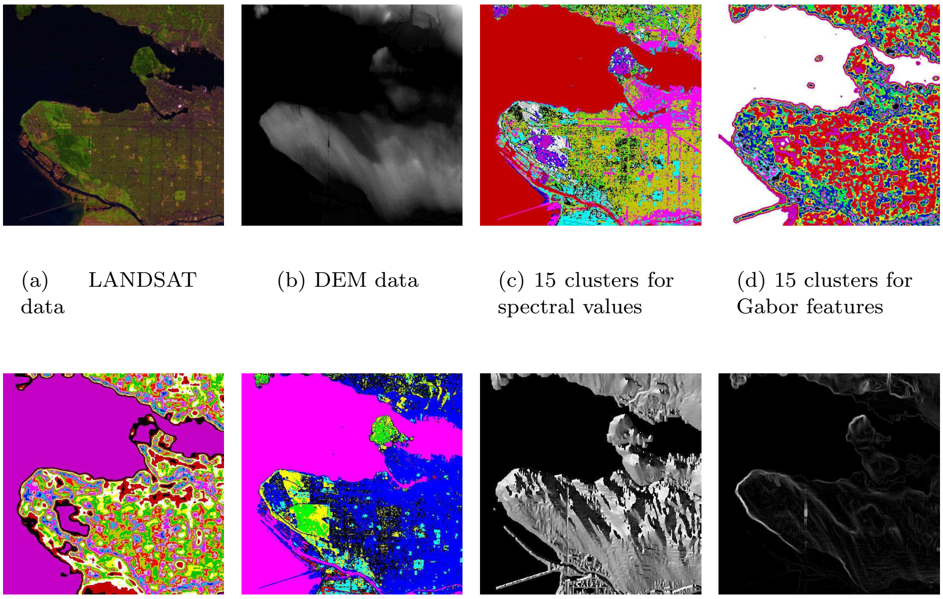

(a) LANDSAT data (b) DEM data (c) 15 clusters for spectral values (d) 15 clusters for Gabor features

(e) 15 clusters for co-occurrence features (f) Spectral mixture analysis (g) Aspect from DEM (h) Slope from DEM

Fig. 1. Raw data and pixel level feature examples for Vancouver, British Columbia. Images in 1(c)-1(f) show the cluster labels for each pixel after unsupervised clustering. Images in 1(g)-1(h) show features computed from DEM data using 3×3 windows around each pixel. These pixel level features are used to compute structural relationships for image classification and retrieval.

semantic class is computed as a combination of its attributes using the Bayes rule (e.g. probability of a region being a residential area given its spectral data, texture features and DEM data). Figures 2(b) and 2(d) show examples for labels assigned to regions using the maximum *a posteriori* probability rule.

2.4. *Spatial Relationships*

The last level in the hierarchy is scene modeling in terms of the spatial relationships of regions. Two scenes with similar regions can have very different interpretations if the regions have different spatial arrangements. Our visual grammar uses region labels identified using supervised and unsupervised classification, and fuzzy modeling of pairwise spatial relationships to describe high-level user concepts (e.g. bordering, invading, surrounding, near, far, right, left, above, below). Fuzzy membership functions for each relationship are constructed based on measurements like region perimeters, shape moments and orientations. When the area of interest consists of multiple regions, the region group is decomposed into region pairs and fuzzy logic

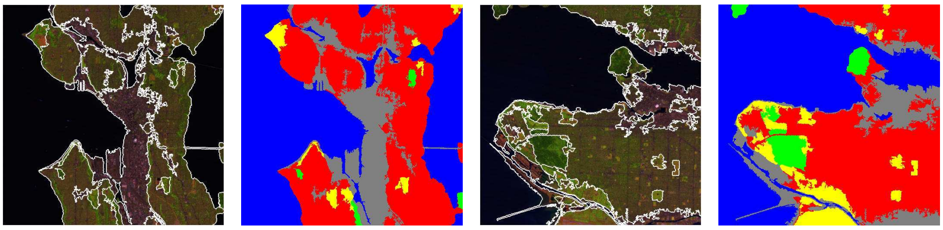

(a) Bayesian segmentation for Seattle

(b) Region labels for Seattle

(c) Bayesian segmentation for Vancouver

(d) Region labels for Vancouver

Fig. 2. Region level representation examples for Seattle, Washington and Vancouver, British Columbia. Segmentation boundaries are marked as white. Region labels are city (gray), field (yellow), green park (lime), residential area (red) and water (blue).

is used to combine the measurements on individual pairs.

Combinations of pairwise relationships enable creation of higher level structures that cannot be modeled by individual pixels or regions. For example, an airport consists of buildings, runways and fields around them. An example airport scene and the automatically recognized region labels are shown in Fig. 3. As discussed in Sec. 1, other examples include a landing zone scene which may be modeled in terms of the interactions between flat regions and surrounding hills, public health studies to find residential areas close to swamp areas, and environmental studies to find forests near water sources. The rest of the chapter describes the details of the visual grammar.

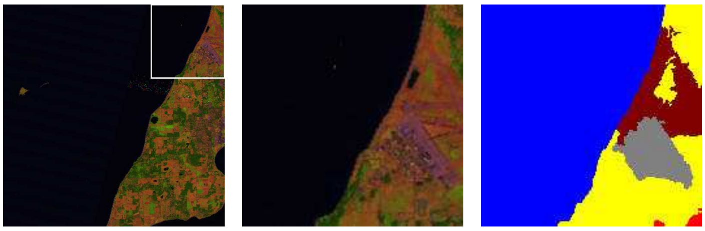

(a) LANDSAT image

(b) Airport zoomed

(c) Region labels

Fig. 3. Modeling of an airport scene in terms of the interactions of its regions. Region labels are dry grass (maroon), buildings and runways (gray), field (yellow), residential area (red), water (blue).

3. Prototype Regions

The first step to construct a visual grammar is to find meaningful and representative regions in an image. Automatic extraction of regions is required to handle large amounts of data. To mimic the identification of regions by experts, we define the concept of prototype regions. A prototype region is a region that has a relatively uniform low-level pixel feature distribution and describes a simple scene or part of a scene. Spectral values or any pixel-level feature listed in Sec. 2.2 can be used for region segmentation. Ideally, a prototype is frequently found in a specific class of scenes and differentiates this class of scenes from others. In addition, using prototypes reduces the possible number of associations between regions and makes the combinatorial problem of region matching more tractable. (This will be discussed in detail in Secs. 5 and 6.)

VisiMine uses unsupervised k-means and model-based clustering to automate the process of finding prototypes. Before unsupervised clustering, image segmentation is used to find regions in images. Interesting prototypes in remote sensing images can be cities, rivers, lakes, residential areas, tidal flats, forests, fields, snow, clouds, etc. Figure 4 shows example prototype regions for different LANDSAT images. The following sections describe the algorithms to find prototype regions in an image collection.

3.1. *K-means Clustering*

K-means clustering[8] is an unsupervised algorithm that partitions the input sample into k clusters by iteratively minimizing a squared-error criterion function. Clusters are represented by the means of the feature vectors associated with each cluster.

In k-means clustering the input parameter k has to be supplied by the user. Once the training data is partitioned into k groups, the prototypes are represented by the cluster means. Then, Euclidean distance in the feature space is used to match regions to prototypes. The degree of match, τ_{ij}, between region i and prototype j is computed as

$$\tau_{ij} = \begin{cases} 1 & \text{if } j = \arg\min_{t=1,\ldots,k} \|\mathbf{x}_i - \boldsymbol{\mu}_t\|^2 \\ 0 & \text{otherwise} \end{cases} \tag{1}$$

where $\mathbf{x}_i$ is the feature vector for region i and $\boldsymbol{\mu}_t$ is the mean vector for cluster t.

3.2. *Model-based Clustering*

Model-based clustering[8] is also an unsupervised algorithm to partition the input sample. In this case, clusters are represented by parametric density models. Parametric density estimation methods assume a specific form for the density function and the problem reduces to finding the estimates of the parameters of this specific form. However, the assumed form can be quite different from the true density. On

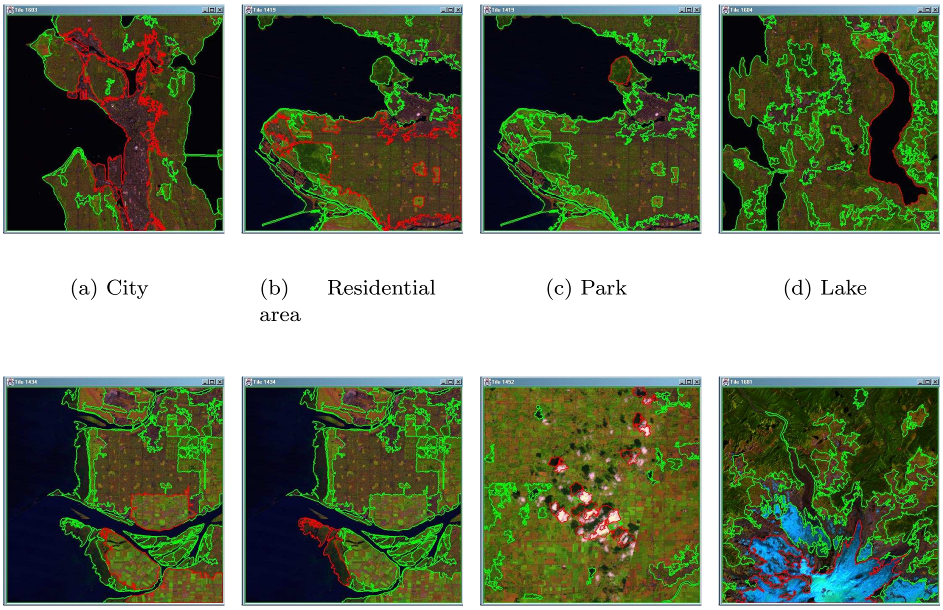

(a) City

(b) Residential area

(c) Park

(d) Lake

(e) Fields

(f) Tidal flat

(g) Clouds and shadows

(h) Glacier

Fig. 4. Example prototype regions for different LANDSAT images. Segmentation boundaries are marked as green and prototype regions are marked as red.

the other hand, non-parametric approaches usually require a large amount of training data and computations can be quite demanding when the data size increases. Mixture models can be used to combine the advantages of both parametric and non-parametric approaches. In a mixture model with k components, the probability of a feature vector $\mathbf{x}$ is defined as

$$p(\mathbf{x}) = \sum_{j=1}^{k} \alpha_j p(\mathbf{x}|j) \tag{2}$$

where α_j is the mixture weight and $p(\mathbf{x}|j)$ is the density model for the j'th component. Mixture models can be considered as semi-parametric models that are not necessarily restricted to a particular density form but also have a fixed number of parameters independent of the size of the data set.

The most commonly used mixture model is the Gaussian mixture with the component densities defined as

$$p(\mathbf{x}|j) = \frac{1}{(2\pi)^{q/2}|\boldsymbol{\Sigma}_{\boldsymbol{j}}|^{1/2}} e^{-(\mathbf{x}-\boldsymbol{\mu}_{\boldsymbol{j}})^T \boldsymbol{\Sigma}_{\boldsymbol{j}}^{-1}(\mathbf{x}-\boldsymbol{\mu}_{\boldsymbol{j}})/2} \tag{3}$$

where $\boldsymbol{\mu}_{\boldsymbol{j}}$ is the mean vector and $\boldsymbol{\Sigma}_{\boldsymbol{j}}$ is the covariance matrix for the j'th component respectively, and q is the dimension of the feature space, $\mathbf{x} \in \mathbb{R}^q$. The Expectation-Maximization (EM) algorithm[27] can be used to estimate the parameters of a mixture. The EM algorithm first finds the expected value of the data log-likelihood using the current parameter estimates (expectation step). Then, the algorithm maximizes this expectation (maximization step). These two steps are repeated iteratively. Each iteration is guaranteed to increase the log-likelihood and the algorithm is guaranteed to converge to a local maximum of the likelihood function.[27]

The iterations for the EM algorithm proceed by using the current estimates as the initial estimates for the next iteration. The k-means algorithm can be used to determine the initial configuration. The mixture weights are computed from the proportion of examples belonging to each cluster. The means are the cluster means. The covariance matrices are calculated as the sample covariance of the points associated with each cluster. Closed form solutions of the EM algorithm for different covariance structures[6,1] are given in Table 1. As a stopping criterion for the EM algorithm, we can use a threshold for the number of iterations or we can stop if the change in log-likelihood between two iterations is less than a threshold.

Table 1. Solutions of the Expectation-Maximization algorithm for a mixture of k Gaussians. $\mathbf{x_1}, \ldots, \mathbf{x_n}$ are training feature vectors independent and identically distributed with $p(\mathbf{x})$ as defined in Eq. (2). Covariance structures used are: $\boldsymbol{\Sigma_j} = \sigma^2\mathbf{I}$, all components having the same spherical covariance matrix; $\boldsymbol{\Sigma_j} = \sigma_j^2\mathbf{I}$, each component having an individual spherical covariance matrix; $\boldsymbol{\Sigma_j} = \mathrm{diag}(\{\sigma_{jt}^2\}_{t=1}^q)$, each component having an individual diagonal covariance matrix; $\boldsymbol{\Sigma_j} = \boldsymbol{\Sigma}$, each component having the same full covariance matrix; $\boldsymbol{\Sigma_j}$, each component having an individual full covariance matrix.

Variable	Estimate
$p(j\|\mathbf{x_i})$	$\frac{\alpha_j p(\mathbf{x_i}\|j)}{\sum_{t=1}^k \alpha_t p(\mathbf{x_i}\|t)}$
$\hat{\alpha}_j$	$\frac{\sum_{i=1}^n p(j\|\mathbf{x_i})}{n}$
$\hat{\boldsymbol{\mu}}_{\boldsymbol{j}}$	$\frac{\sum_{i=1}^n p(j\|\mathbf{x_i})\mathbf{x_i}}{\sum_{i=1}^n p(j\|\mathbf{x_i})}$
$\hat{\boldsymbol{\Sigma}}_{\boldsymbol{j}} = \hat{\sigma}^2\mathbf{I}$	$\hat{\sigma}^2 = \frac{\sum_{j=1}^k \sum_{i=1}^n p(j\|\mathbf{x_i})(\mathbf{x_i}-\hat{\boldsymbol{\mu}}_{\boldsymbol{j}})^T(\mathbf{x_i}-\hat{\boldsymbol{\mu}}_{\boldsymbol{j}})}{nq}$
$\hat{\boldsymbol{\Sigma}}_{\boldsymbol{j}} = \hat{\sigma}_j^2\mathbf{I}$	$\hat{\sigma}_j^2 = \frac{\sum_{i=1}^n p(j\|\mathbf{x_i})(\mathbf{x_i}-\hat{\boldsymbol{\mu}}_{\boldsymbol{j}})^T(\mathbf{x_i}-\hat{\boldsymbol{\mu}}_{\boldsymbol{j}})}{q\sum_{i=1}^n p(j\|\mathbf{x_i})}$
$\hat{\boldsymbol{\Sigma}}_{\boldsymbol{j}} = \mathrm{diag}(\{\hat{\sigma}_{jt}^2\}_{t=1}^q)$	$\hat{\sigma}_{jt}^2 = \frac{\sum_{i=1}^n p(j\|\mathbf{x_i})(\mathbf{x}_{\boldsymbol{i}t}-\hat{\boldsymbol{\mu}}_{\boldsymbol{j}t})^2}{\sum_{i=1}^n p(j\|\mathbf{x_i})}$
$\hat{\boldsymbol{\Sigma}}_{\boldsymbol{j}} = \hat{\boldsymbol{\Sigma}}$	$\hat{\boldsymbol{\Sigma}} = \frac{\sum_{j=1}^k \sum_{i=1}^n p(j\|\mathbf{x_i})(\mathbf{x_i}-\hat{\boldsymbol{\mu}}_{\boldsymbol{j}})(\mathbf{x_i}-\hat{\boldsymbol{\mu}}_{\boldsymbol{j}})^T}{n}$
$\hat{\boldsymbol{\Sigma}}_{\boldsymbol{j}}$, full	$\hat{\boldsymbol{\Sigma}}_{\boldsymbol{j}} = \frac{\sum_{i=1}^n p(j\|\mathbf{x_i})(\mathbf{x_i}-\hat{\boldsymbol{\mu}}_{\boldsymbol{j}})(\mathbf{x_i}-\hat{\boldsymbol{\mu}}_{\boldsymbol{j}})^T}{\sum_{i=1}^n p(j\|\mathbf{x_i})}$

The number of components in the mixture can be either supplied by the user or chosen using optimization criteria like the Minimum Description Length Principle.[31,1] Once the mixture parameters are computed, each component corresponds to a prototype. The degree of match, τ_{ij}, between region i and prototype j becomes the posterior probability $\tau_{ij} = p(j|\mathbf{x_i})$. The maximum *a posteriori* probability (MAP) rule is used to match regions to prototypes where region i is assigned to prototype j^* as

$$\begin{aligned} j^* &= \arg \max_{j=1,\ldots,k} p(j|\mathbf{x}_{\boldsymbol{i}}) \\ &= \arg \max_{j=1,\ldots,k} \alpha_j p(\mathbf{x}_{\boldsymbol{i}}|j) \\ &= \arg \max_{j=1,\ldots,k} \log(\alpha_j p(\mathbf{x}_{\boldsymbol{i}}|j)) \\ &= \arg \max_{j=1,\ldots,k} \left\{ \log \alpha_j - \frac{1}{2} \log |\boldsymbol{\Sigma}_{\boldsymbol{j}}| - \frac{1}{2} (\mathbf{x}_{\boldsymbol{i}} - \boldsymbol{\mu}_{\boldsymbol{j}})^T \boldsymbol{\Sigma}_{\boldsymbol{j}}^{-1} (\mathbf{x}_{\boldsymbol{i}} - \boldsymbol{\mu}_{\boldsymbol{j}}) \right\} . \end{aligned} \tag{4}$$

4. Region Relationships

After the regions in the database are clustered into groups of prototype regions, the next step in the construction of the visual grammar is modeling of their spatial relationships. The following sections describe how relationships of region pairs and their combinations can be computed to describe high-level user concepts.

4.1. *Second-order Region Relationships*

Second-order region relationships consist of the relationships between region pairs. These pairs can occur in the image in many possible ways. However, the regions of interest are usually the ones that are close to each other. Representations of spatial relationships depend on the representations of regions. VisiMine models regions by their boundary pixels and moments. Other possible representations include minimum bounding rectangles,[37] Fourier descriptors[33] and graph-based approaches.[29]

The spatial relationships between all region pairs in an image can be represented by a region relationship matrix. To find the relationship between a pair of regions represented by their boundary pixels and moments, we first compute

- perimeter of the first region, π_i
- perimeter of the second region, π_j
- common perimeter between two regions, π_{ij}
- ratio of the common perimeter to the perimeter of the first region, $r_{ij} = \frac{\pi_{ij}}{\pi_i}$
- closest distance between the boundary pixels of the first region and the boundary pixels of the second region, d_{ij}
- centroid of the first region, ν_i
- centroid of the second region, ν_j
- angle between the horizontal (column) axis and the line joining the centroids, θ_{ij}

where $i, j \in \{1, \ldots, n\}$ and n is the number of regions in the image.

The distance d_{ij} is computed using the distance transform.[11] Given a particular region $\mathcal{A}$, to each pixel that is not in $\mathcal{A}$, the distance transform assigns a number that is the spatial distance between that pixel and $\mathcal{A}$. Then, the distance between region $\mathcal{A}$ and another region $\mathcal{B}$ is the smallest distance transform value for the boundary pixels of $\mathcal{B}$. The angle θ_{ij} is computed as

$$\theta_{ij} = \begin{cases} \arccos\left(\frac{\nu_{ic}-\nu_{jc}}{d_{ij}}\right) & \text{if } \nu_{ir} \geq \nu_{jr} \\ -\arccos\left(\frac{\nu_{ic}-\nu_{jc}}{d_{ij}}\right) & \text{otherwise} \end{cases} \tag{5}$$

where ν_{ir} and ν_{ic} are the row and column coordinates of the centroid of region i, respectively (see Fig. 5 for illustrations). Then, the $n \times n$ region relationship matrix is defined as

$$\mathbf{R} = \{\{r_{ij}, d_{ij}, \theta_{ij}\} \,|\, i, j = 1, \ldots, n, \ \forall i \neq j\}\,. \tag{6}$$

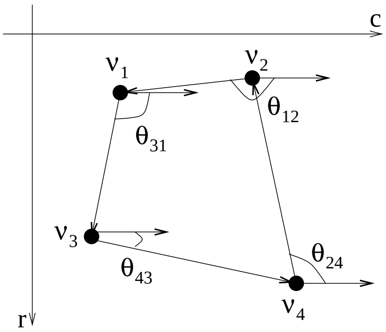

Fig. 5. Orientation of two regions is computed using the angle between the horizontal (column) axis and the line joining their centroids. In the examples above, θ_{ij} is the angle between the c-axis and the line directed from the second centroid ν_j to the first centroid ν_i. It is used to compute the orientation of region i with respect to region j. θ_{ij} increases in the clockwise direction, in this case $\theta_{24} < 0 < \theta_{43} < \theta_{31} < \theta_{12}$.

One way to define the spatial relationships between regions i and j is to use crisp (Boolean) decisions about r_{ij}, d_{ij} and θ_{ij}. Another way is to define them as relationship classes.[33] Each region pair can be assigned a degree of their spatial relationship using fuzzy class membership functions. Denote the class membership functions by Ω_c with $c \in \{\mathsf{DIS}, \mathsf{BOR}, \mathsf{INV}, \mathsf{SUR}, \mathsf{NEAR}, \mathsf{FAR}, \mathsf{RIGHT}, \mathsf{LEFT}, \mathsf{ABOVE}, \mathsf{BELOW}\}$ corresponding to *disjoined*, *bordering*, *invaded_by*, *surrounded_by*, *near*, *far*, *right*, *left*, *above* and *below*, respectively. Then, the value $\Omega_c(r_{ij}, d_{ij}, \theta_{ij})$ represents the degree of membership of regions i and j to class c.

Among the above, *disjoined*, *bordering*, *invaded_by* and *surrounded_by* are perimeter-class relationships, *near* and *far* are distance-class relationships, and *right*, *left*, *above* and *below* are orientation-class relationships. These relationships are divided into sub-groups because multiple relationships can be used to describe a region pair, e.g. *invaded_by* from *left*, *bordering* from *above*, and *near* and *right*, etc. Illustrations are given in Fig. 6.

For the perimeter-class relationships, we use the perimeter ratios r_{ij} with the following trapezoid membership functions:

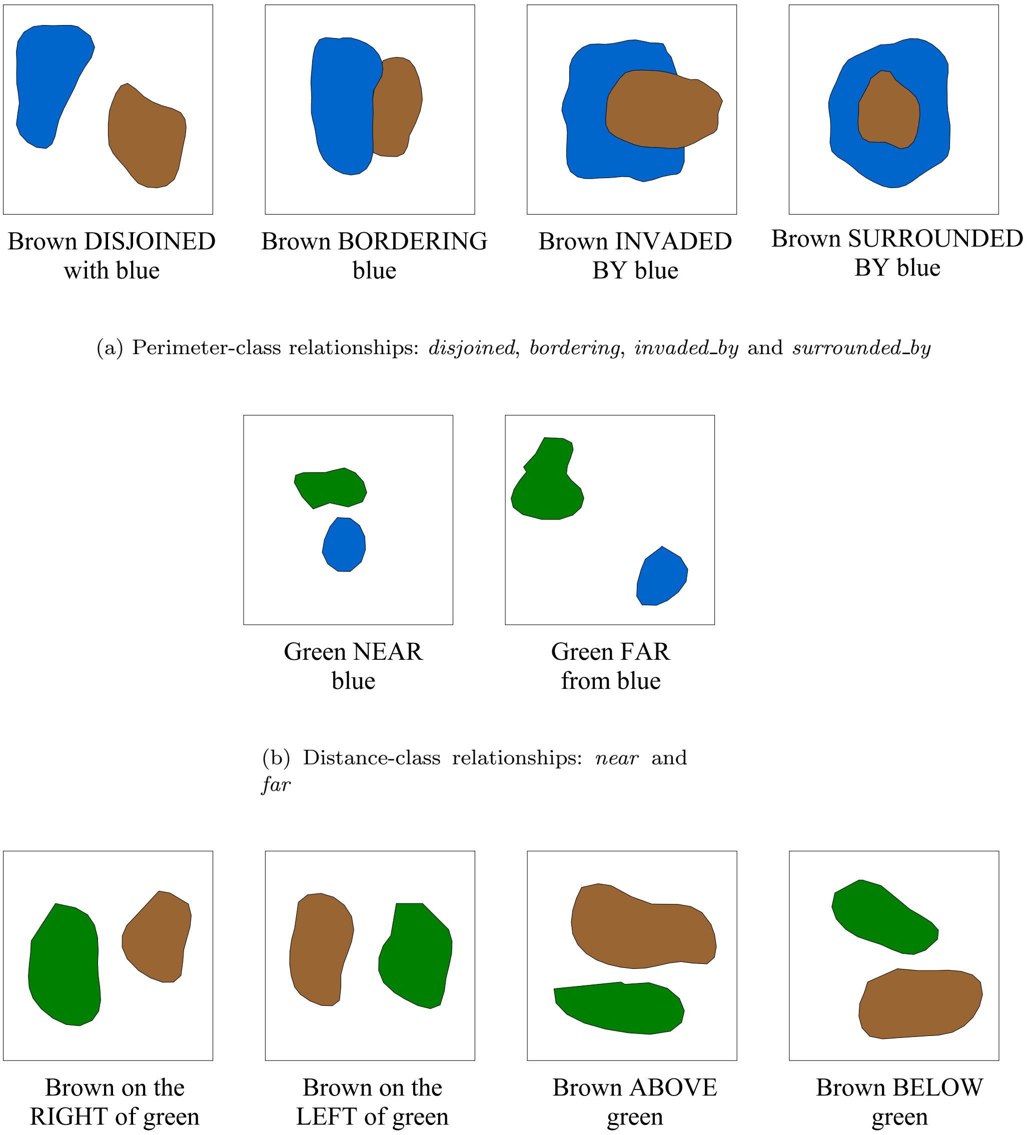

(a) Perimeter-class relationships: *disjoined*, *bordering*, *invaded_by* and *surrounded_by*

(b) Distance-class relationships: *near* and *far*

(c) Orientation-class relationships: *right*, *left*, *above* and *below*

Fig. 6. Spatial relationships of region pairs.

- *disjoined*:

$$\Omega_{\mathsf{DIS}}(r_{ij}) \triangleq \begin{cases} 1 & \text{if } r_{ij} = 0 \\ 0 & \text{otherwise.} \end{cases} \tag{7}$$

- *bordering*:

$$\Omega_{\mathsf{BOR}}(r_{ij}) \triangleq \begin{cases} 1 & \text{if } 0 < r_{ij} \leq 0.40 \\ -\frac{20}{13} r_{ij} + \frac{21}{13} & \text{if } 0.40 < r_{ij} \leq 1 \\ 0 & \text{otherwise.} \end{cases} \tag{8}$$

- *invaded_by*:

$$\Omega_{\mathsf{INV}}(r_{ij}) \triangleq \begin{cases} 10 r_{ij} - 4 & \text{if } 0.40 \leq r_{ij} < 0.50 \\ 1 & \text{if } 0.50 \leq r_{ij} \leq 0.80 \\ -\frac{10}{3} r_{ij} + \frac{11}{3} & \text{if } 0.80 < r_{ij} \leq 1 \\ 0 & \text{otherwise.} \end{cases} \tag{9}$$

- *surrounded_by*:

$$\Omega_{\mathsf{SUR}}(r_{ij}) \triangleq \begin{cases} \frac{20}{3} r_{ij} - \frac{16}{3} & \text{if } 0.80 \leq r_{ij} < 0.95 \\ 1 & \text{if } 0.95 \leq r_{ij} \leq 1 \\ 0 & \text{otherwise.} \end{cases} \tag{10}$$

These functions are shown in Fig. 7(a). The motivation for the choice of these functions is as follows. Two regions are disjoined when they are not touching each other. They are bordering each other when they have a common perimeter. When the common perimeter between two regions gets closer to 50%, the larger region starts invading the smaller one. When the common perimeter goes above 80%, the relationship is considered an almost complete invasion, i.e. surrounding.

For the distance-class relationships, we use the perimeter ratios r_{ij}, distances between region boundaries d_{ij} and sigmoid membership functions with the constraint $\Omega_{\mathsf{NEAR}}(r_{ij}, d_{ij}) + \Omega_{\mathsf{FAR}}(r_{ij}, d_{ij}) = 1$. The membership functions are defined as:

- *near*:

$$\Omega_{\mathsf{NEAR}}(r_{ij}, d_{ij}) \triangleq \begin{cases} 1 & \text{if } r_{ij} > 0 \\ \frac{e^{-\alpha(d_{ij}-\beta)}}{1+e^{-\alpha(d_{ij}-\beta)}} & \text{otherwise.} \end{cases} \tag{11}$$

- *far*:

$$\Omega_{\mathsf{FAR}}(r_{ij}, d_{ij}) \triangleq \begin{cases} 0 & \text{if } r_{ij} > 0 \\ \frac{1}{1+e^{-\alpha(d_{ij}-\beta)}} & \text{otherwise.} \end{cases} \tag{12}$$

These functions are shown in Fig. 7(b). β is the parameter that determines the cut-off value when a region becomes more far than near, and α is the parameter that determines the crispness of the function. We first choose β to be a quarter of the image width, i.e. $\beta = 0.25w$ where w is the image width, and then choose α to give a *far* fuzzy membership value less than 0.01 at distance 0, i.e. $\frac{1}{1+e^{\alpha\beta}} < 0.01 \Rightarrow \alpha > \log(99)/\beta$.

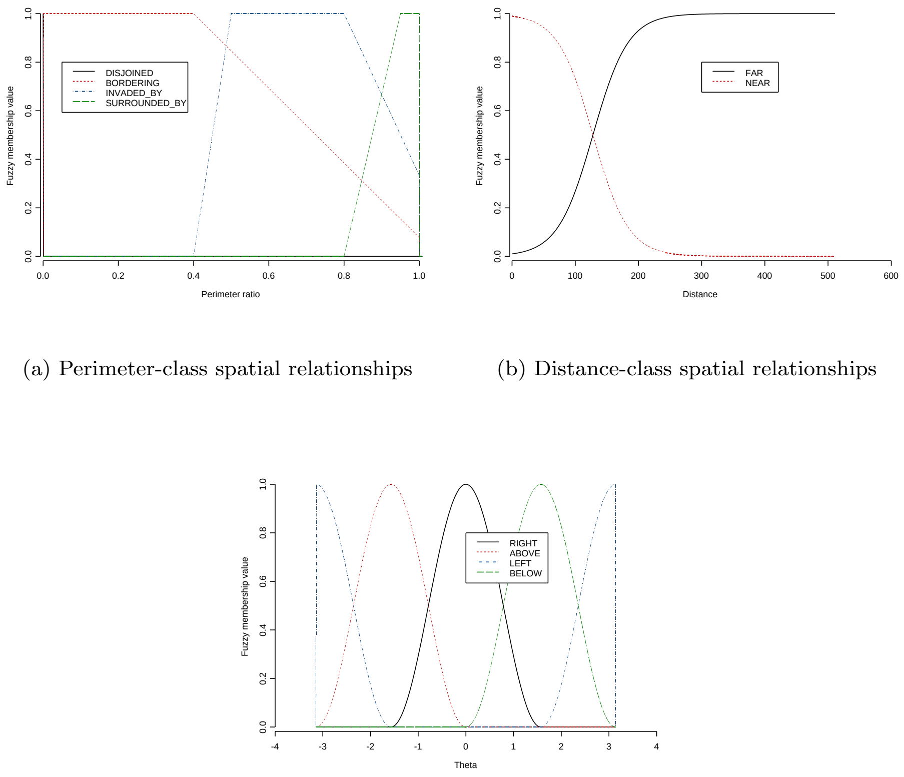

(a) Perimeter-class spatial relationships

(b) Distance-class spatial relationships

(c) Orientation-class spatial relationships

Fig. 7. Fuzzy membership functions for pairwise spatial relationships.

For the orientation-class relationships, we use the angles θ_{ij} and truncated cosine membership functions with the constraint $\Omega_{\mathsf{RIGHT}}(\theta_{ij}) + \Omega_{\mathsf{LEFT}}(\theta_{ij}) + \Omega_{\mathsf{ABOVE}}(\theta_{ij}) + \Omega_{\mathsf{BELOW}}(\theta_{ij}) = 1$. The membership functions are defined as:

- *right*:

$$\Omega_{\mathsf{RIGHT}}(\theta_{ij}) \triangleq \begin{cases} \frac{1+\cos(2\theta_{ij})}{2} & \text{if } -\pi/2 < \theta_{ij} < \pi/2 \\ 0 & \text{otherwise.} \end{cases} \tag{13}$$

- *left*:

$$\Omega_{\mathsf{LEFT}}(\theta_{ij}) \triangleq \begin{cases} \frac{1+\cos(2\theta_{ij})}{2} & \text{if } -\pi < \theta_{ij} < -\pi/2 \text{ or } \pi/2 < \theta_{ij} < \pi \\ 0 & \text{otherwise.} \end{cases} \tag{14}$$

- *above*:

$$\Omega_{\mathsf{ABOVE}}(\theta_{ij}) \triangleq \begin{cases} \frac{1-\cos(2\theta_{ij})}{2} & \text{if } -\pi < \theta_{ij} < 0 \\ 0 & \text{otherwise.} \end{cases} \tag{15}$$

- *below*:

$$\Omega_{\mathsf{BELOW}}(\theta_{ij}) \triangleq \begin{cases} \frac{1-\cos(2\theta_{ij})}{2} & \text{if } 0 < \theta_{ij} < \pi \\ 0 & \text{otherwise.} \end{cases} \tag{16}$$

These functions are shown in Fig. 7(c).

Note that the pairwise relationships are not always symmetric, i.e. $\Omega_c(r_{ij}, d_{ij}, \theta_{ij})$ is not necessarily equal to $\Omega_c(r_{ji}, d_{ji}, \theta_{ji})$. Furthermore, some relationships are stronger than others. For example, *surrounded_by* is stronger than *invaded_by*, and *invaded_by* is stronger than *bordering*, e.g. the relationship "small region *invaded_by* large region" is preferred over the relationship "large region *bordering* small region". The class membership functions are chosen so that only one of them is the largest for a given set of measurements $r_{ij}, d_{ij}, \theta_{ij}$. We label a region pair as having the perimeter-class, distance-class and orientation-class relationships

$$\begin{aligned} c^1_{ij} &= \operatorname*{arg\,max}_{c\in\{\mathsf{DIS,BOR,INV,SUR}\}} \Omega_c(r_{ij}, d_{ij}, \theta_{ij}) \\ c^2_{ij} &= \operatorname*{arg\,max}_{c\in\{\mathsf{NEAR,FAR}\}} \Omega_c(r_{ij}, d_{ij}, \theta_{ij}) \\ c^3_{ij} &= \operatorname*{arg\,max}_{c\in\{\mathsf{RIGHT,LEFT,ABOVE,BELOW}\}} \Omega_c(r_{ij}, d_{ij}, \theta_{ij}) \end{aligned} \tag{17}$$

with the corresponding degrees

$$\rho^t_{ij} = \Omega_{c^t_{ij}}(r_{ij}, d_{ij}, \theta_{ij}), \quad t = 1, 2, 3. \tag{18}$$

4.2. *Higher-order Region Relationships*

Higher-order relationships (of region groups) can be decomposed into multiple second-order relationships (of region pairs). Therefore, the measures defined in the previous section can be computed for each of the pairwise relationships and can be combined to measure the combined relationship. The equivalent of the Boolean "and" operation in fuzzy logic is the "min" operation. For a combination of k regions, there are $\binom{k}{2} = \frac{k(k-1)}{2}$ pairwise relationships. Therefore, the relationship between these k regions can be represented as lists of $\binom{k}{2}$ pairwise relationships using Eq. (17) as

$$c^t_{1\dots k} = \{c^t_{ij} \,|\, i, j = 1, \dots, k, \ \forall i < j\}, \quad t = 1, 2, 3 \tag{19}$$

with the corresponding degrees computed using Eq. (18) as

$$\rho^t_{1\dots k} = \min_{\substack{i,j=1,\dots,k \\ i<j}} \rho^t_{ij}, \quad t = 1, 2, 3. \tag{20}$$

Example decompositions are given in Fig. 8. These examples show scenarios that cannot be described by conventional region or scene level image analysis algorithms which assume the regions or scenes consist of pixels with similar feature characteristics.

5. Image Retrieval

To use the automatically built visual grammar models for image mining, users can compose queries for complex scene scenarios by giving a set of example regions or by selecting an area of interest in a scene. VisiMine encodes and searches for a query scene with multiple regions using the visual grammar as follows:

(1) Let k be the number of regions selected by the user. Find the prototype label for each of the k regions.

(2) Find the perimeter ratio, distance and orientation for each of the $\binom{k}{2}$ possible region pairs.

(3) Find the spatial relationship and its degree for these k regions using Eqs. (19) and (20). Denote them by $\bar{c}^t = \{\bar{c}^t_{ij} \,|\, i,j = 1,\ldots,k,\ \forall i < j\}, t = 1,2,3$ and $\bar{\rho}^t, t = 1,2,3$, respectively.

(4) For each image in the database,

   (a) For each query region, find the list of regions with the same prototype label as itself. Denote these lists by $U_i, i = 1,\ldots,k$. These regions are the candidate matches to query regions. Using previously defined prototype labels simplifies region matching into a table look-up process instead of expensive similarity computations between region features.

   (b) Rank region groups $(u_1, u_2, \ldots, u_k) \in U_1 \times U_2 \times \cdots \times U_k$ according to the distance

$$\left| \min_{t=1,2,3} \bar{\rho}^t - \min_{t=1,2,3} \min_{\substack{i,j=1,\ldots,k \\ i<j}} \Omega_{\bar{c}^t_{ij}}(r_{u_i u_j}, d_{u_i u_j}, \theta_{u_i u_j}) \right| \tag{21}$$

   or alternatively according to

$$\max_{t=1,2,3} \max_{\substack{i,j=1,\ldots,k \\ i<j}} \left| \bar{\rho}^t_{ij} - \Omega_{\bar{c}^t_{ij}}(r_{u_i u_j}, d_{u_i u_j}, \theta_{u_i u_j}) \right|. \tag{22}$$

   (c) The equivalent of the Boolean "or" operation in fuzzy logic is the "max" operation. To rank image tiles, use the distance

$$\left| \min_{t=1,2,3} \bar{\rho}^t - \max_{\substack{(u_1,u_2,\ldots,u_k)\in \\ U_1\times U_2\times\cdots\times U_k}} \left\{ \min_{t=1,2,3} \min_{\substack{i,j=1,\ldots,k \\ i<j}} \Omega_{\bar{c}^t_{ij}}(r_{u_i u_j}, d_{u_i u_j}, \theta_{u_i u_j}) \right\} \right| \tag{23}$$

   or alternatively the distance

$$\min_{\substack{(u_1,u_2,\ldots,u_k)\in \\ U_1\times U_2\times\cdots\times U_k}} \left\{ \max_{t=1,2,3} \max_{\substack{i,j=1,\ldots,k \\ i<j}} \left| \bar{\rho}^t_{ij} - \Omega_{\bar{c}^t_{ij}}(r_{u_i u_j}, d_{u_i u_j}, \theta_{u_i u_j}) \right| \right\}. \tag{24}$$

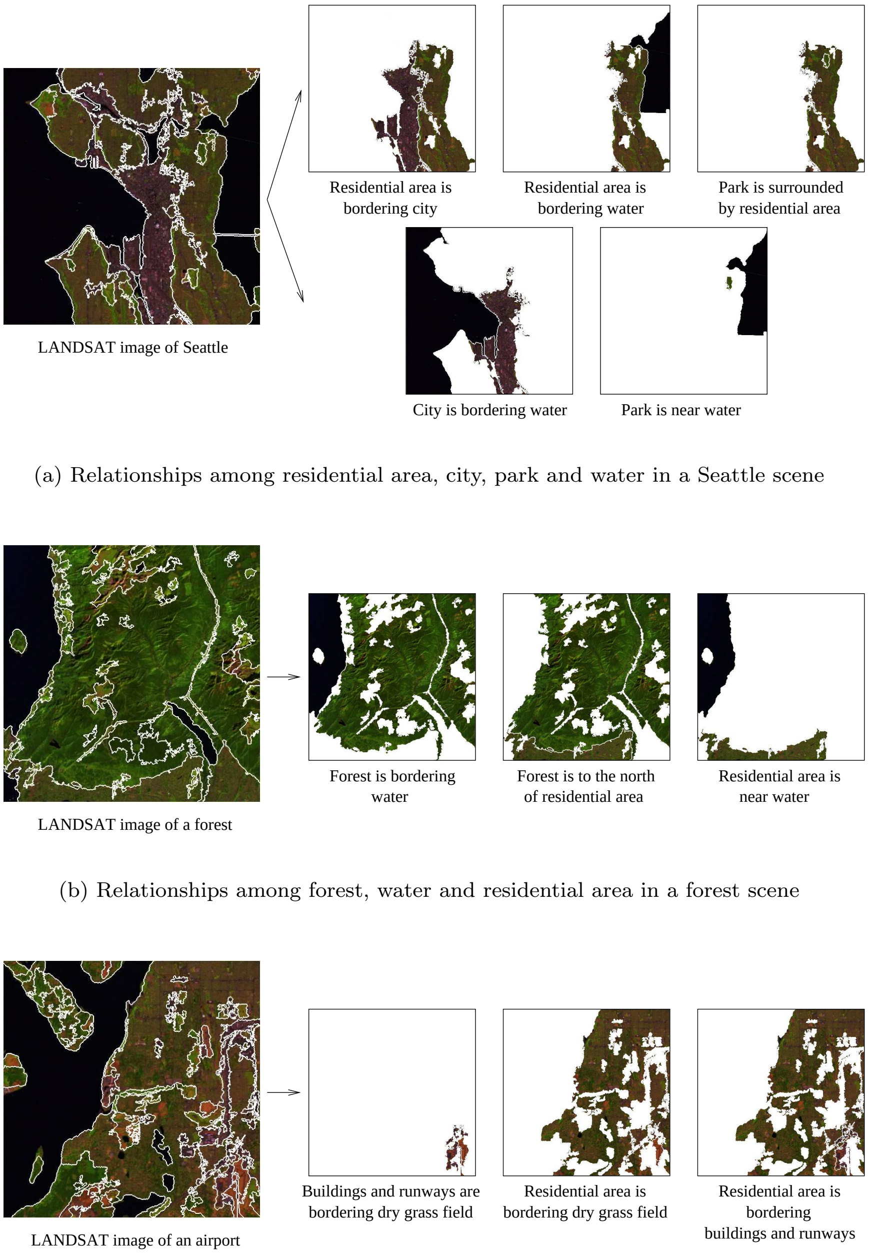
Residential area is bordering city
Residential area is bordering water
Park is surrounded by residential area
LANDSAT image of Seattle
City is bordering water
Park is near water
Forest is bordering water
Forest is to the north of residential area
Residential area is near water
LANDSAT image of a forest
Buildings and runways are bordering dry grass field
Residential area is bordering dry grass field
Residential area is bordering buildings and runways
LANDSAT image of an airport

(a) Relationships among residential area, city, park and water in a Seattle scene

(b) Relationships among forest, water and residential area in a forest scene

(c) Relationships among buildings, runways, dry grass field and residential area in an airport scene

Fig. 8. Example decomposition of scenes into relationships of region pairs. Segmentation boundaries are marked as white.

In some cases, some of the spatial relationships (e.g. *above*, *right*) can be too restrictive. The visual grammar also includes a DONT_CARE relationship class that allows the user to constrain the searches based on the relationship groups he is interested in using the VisiMine graphical user interface. Relevance feedback can also be used to find the most important relationship class (perimeter, distance or orientation) for a particular query.

Example queries on a LANDSAT database covering Washington State in the U.S.A. and southern part of British Columbia in Canada are given in Figs. 9–13. Traditionally, queries that consist of multiple regions are handled by computing a single set of features using all the pixels in the union of those regions. However, this averaging causes a significant information loss because features of pixels in different regions usually correspond to different neighborhoods in the feature space and averaging distorts the multimodal characteristic of the query. For example, averaging features computed from the regions in these query scenes ignores the spatial organization of concrete, soil, grass, trees and water in those scenes. On the other hand, the visual grammar can capture both feature and spatial characteristics of region groups.

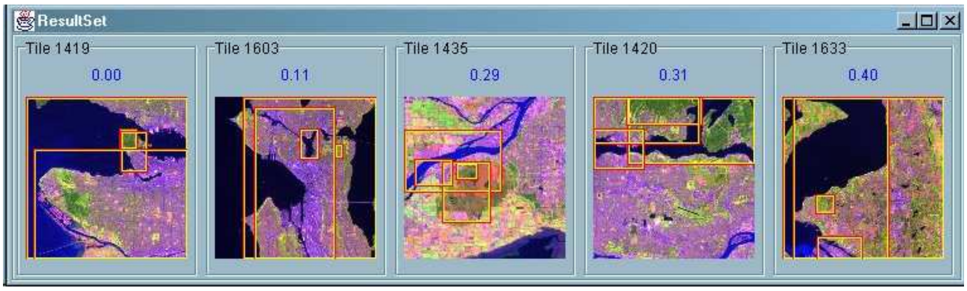

Fig. 9. Search results for a scene where a residential area is bordering a city and both are bordering water, and a park is surrounded by a residential area and is also near water. Identified regions are marked by their minimum bounding rectangles. Decomposition of the query scene is given in Fig. 8(a).

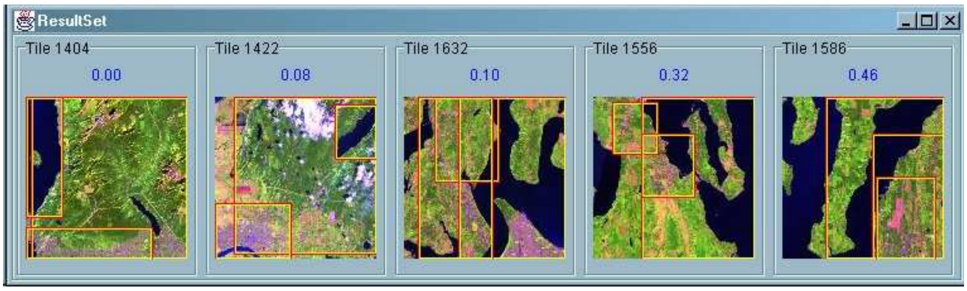

Fig. 10. Search results for a scene where a forest is bordering water and is also to the north of a residential area. Decomposition of the query scene is given in Fig. 8(b).

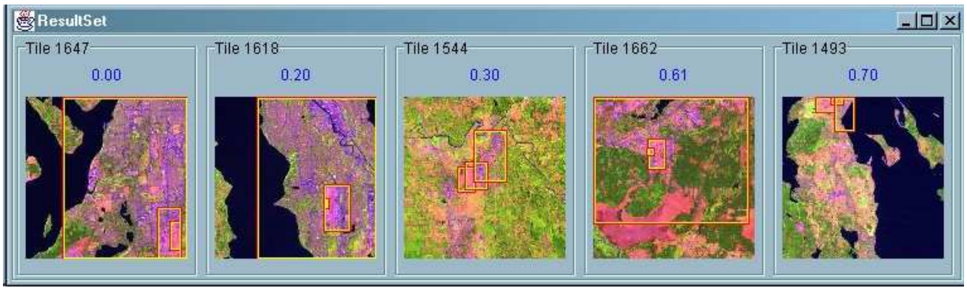

Fig. 11. Search results for a scene where buildings, runways and their neighboring dry grass field are near a residential area. Decomposition of the query scene is given in Fig. 8(c).

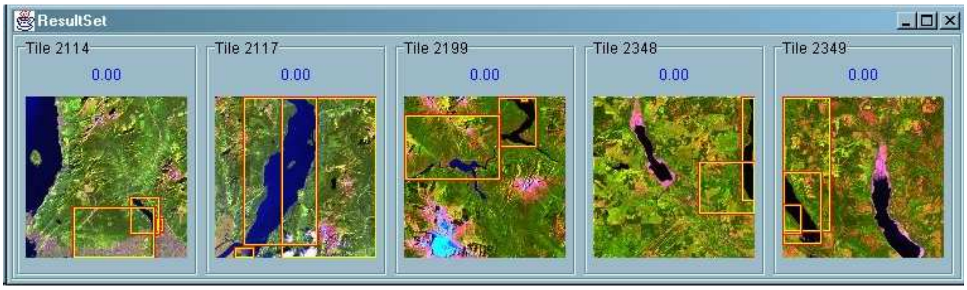

Fig. 12. Search results for a scene where a lake is surrounded by tree covered hills.

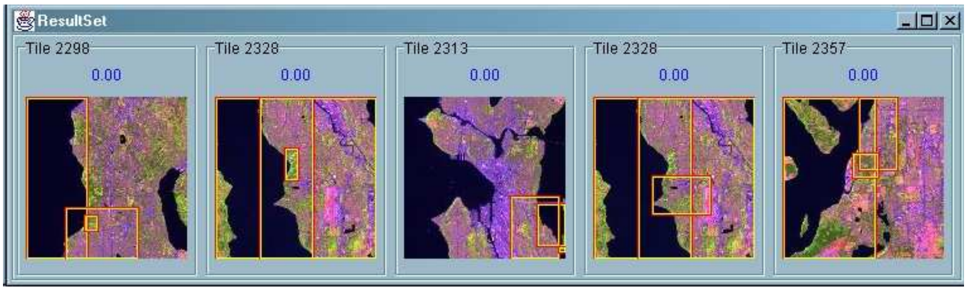

Fig. 13. Search results for a scene where a residential area and its neighboring park are both bordering water.

6. Image Classification

Image classification is defined here as a problem of assigning images to different classes according to the scenes they contain. Commonly used statistical classifiers require a lot of training data to effectively compute the spectral and textural signatures for pixels and also cannot do classification based on high-level user concepts because of the lack of spatial information. Rule-based classifiers also require significant amount of user involvement every time a new class is introduced to the system.

The visual grammar enables creation of higher level classes that cannot be modeled by individual pixels or regions. Furthermore, learning of these classifiers require only a few training images. We use a Bayesian framework that learns scene classes based on automatic selection of distinguishing (e.g. frequently occurring, rarely occurring) relations between regions.

The input to the system is a set of training images that contain example scenes for each class defined by the user. Let s be the number of classes, m be the number of relationships defined for region pairs, k be the number of regions in a region group, and t be a threshold for the number of region groups that will be used in the classifier. Denote the classes by $w_1, \ldots, w_s$. VisiMine automatically builds classifiers from the training data as follows:

(1) Count the number of times each possible region group with a particular spatial relationship is found in the set of training images for each class. This is a combinatorial problem because the total number of region groups (unordered arrangements without replacement) in an image with n regions is $\binom{n}{k}$ and the total number of possible relationships (unordered arrangements with replacement) in a region group is $\binom{m+\binom{k}{2}-1}{\binom{k}{2}}$. A region group of interest is the one that is frequently found in a particular class of scenes but rarely exists in other classes. For each region group, this can be measured using class separability which can be computed in terms of within-class and between-class variances of the counts as

$$\varsigma = \log\left(1 + \frac{\sigma_B^2}{\sigma_W^2}\right) \tag{25}$$

where $\sigma_W^2 = \sum_{i=1}^{s} v_i \mathrm{var}\{z_j \,|\, j \in w_i\}$ is the within-class variance, v_i is the number of training images for class w_i, z_j is the number of times this region group is found in training image j, $\sigma_B^2 = \mathrm{var}\{\sum_{j\in w_i} z_j \,|\, i = 1, \ldots, s\}$ is the between-class variance, and $\mathrm{var}\{\cdot\}$ denotes the variance of a sample.

(2) Select the top t region groups with the largest class separability values. Let $x_1, \ldots, x_t$ be Bernoulli random variables for these region groups, where $x_j = T$ if the region group x_j is found in an image and $x_j = F$ otherwise. Let $p(x_j = T) = \theta_j$. Then, the number of times x_j is found in images from class w_i has a $\mathrm{Binomial}(v_i, \theta_j) = \binom{v_i}{v_{ij}}\theta_j^{v_{ij}}(1-\theta_j)^{v_i - v_{ij}}$ distribution where v_{ij} is the number of training images for w_i that contain x_j. The maximum likelihood estimate of θ_j becomes

$$p(x_j = T|w_i) = \frac{v_{ij}}{v_i}. \tag{26}$$

Using a $\mathrm{Beta}(1,1)$ distribution as the conjugate prior, the Bayes estimate for θ_j is computed as

$$p(x_j = T|w_i) = \frac{v_{ij}+1}{v_i+2}. \tag{27}$$

Using a similar procedure with Multinomial and Dirichlet distributions, the Bayes estimate for an image belonging to class w_i (i.e. containing the scene defined by class w_i) is computed as

$$p(w_i) = \frac{v_i + 1}{\sum_{i=1}^{s} v_i + s}. \tag{28}$$

In other words, discrete probability tables are constructed using v_i and v_{ij}, $i = 1, \ldots, s, j = 1, \ldots, t$, and conjugate priors are used to update them when new images become available via relevance feedback.

(3) For an unknown image, search for each of the t region groups (determine whether $x_j = T$ or $x_j = F$, $\forall j$) and compute the probability for each class using the conditional independence assumption as

$$\begin{aligned} p(w_i|x_1, \ldots, x_t) &= \frac{p(w_i, x_1, \ldots, x_t)}{p(x_1, \ldots, x_t)} \\ &= \frac{p(w_i)p(x_1, \ldots, x_t|w_i)}{p(x_1, \ldots, x_t)} \\ &= \frac{p(w_i)\prod_{j=1}^{t} p(x_j|w_i)}{p(x_1, \ldots, x_t)}. \end{aligned} \tag{29}$$

Assign that image to the best matching class using the MAP rule as

$$\begin{aligned} w^* &= \arg\max_{w_i} p(w_i|x_1, \ldots, x_t) \\ &= \arg\max_{w_i} p(w_i) \prod_{j=1}^{t} p(x_j|w_i). \end{aligned} \tag{30}$$

Classification examples are given in Figs. 14–16. We used four training images for each of the classes defined as “clouds”, “tree covered islands”, “residential areas with a coastline”, “snow covered mountains”, “fields” and “high-altitude forests”. These classes provide a challenge where a mixture of spectral, textural, elevation and spatial information is required for correct identification of the scenes. For example, pixel level classifiers often misclassify clouds as snow and shadows as water. On the other hand, the Bayesian classifier described above could successfully eliminate most of the false alarms by first recognizing regions that belonged to cloud and shadow prototypes and then verified these region groups according to the fact that clouds are often accompanied by their shadows in a LANDSAT scene. Other scene classes like residential areas with a coastline or tree covered islands cannot be identified by pixel level or scene level algorithms that do not use spatial information. The visual grammar classifiers automatically learned the distinguishing region groups that were frequently found in particular classes of scenes but rarely existed in other classes.

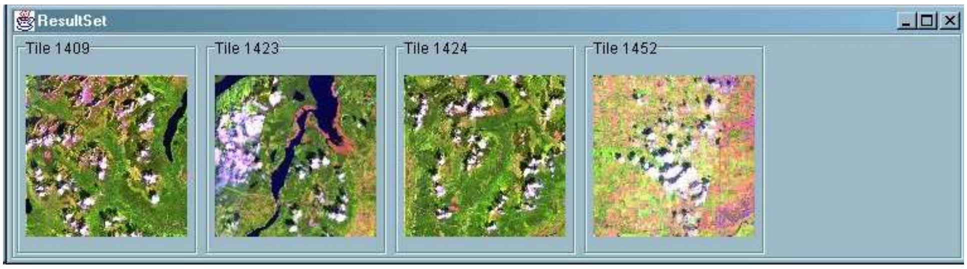

(a) Training images

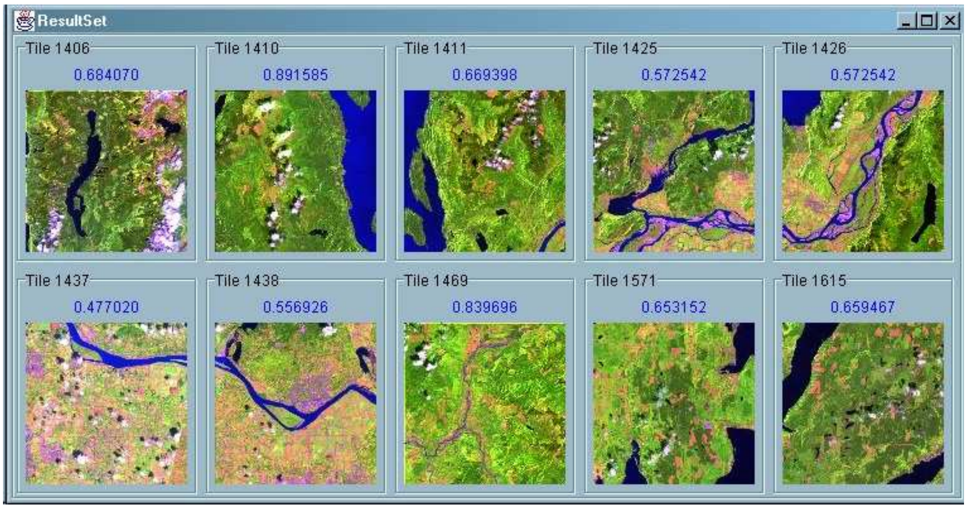

(b) Images classified as containing clouds

Fig. 14. Classification results for the "clouds" class which is automatically modeled by the distinguishing relationships of white regions (clouds) with their neighboring dark regions (shadows).

7. Conclusions

In this chapter we described a probabilistic visual grammar to automatically analyze complex query scenarios using spatial relationships of regions and described algorithms to use it for content-based image retrieval and classification. Our hierarchical scene modeling bridges the gap between feature extraction and semantic interpretation. The approach includes unsupervised clustering to identify prototype regions in images (e.g. city, residential, water, field, forest, glacier), fuzzy modeling of region spatial relationships to describe high-level user concepts (e.g. bordering, surrounding, near, far, above, below), and Bayesian classifiers to learn image classes

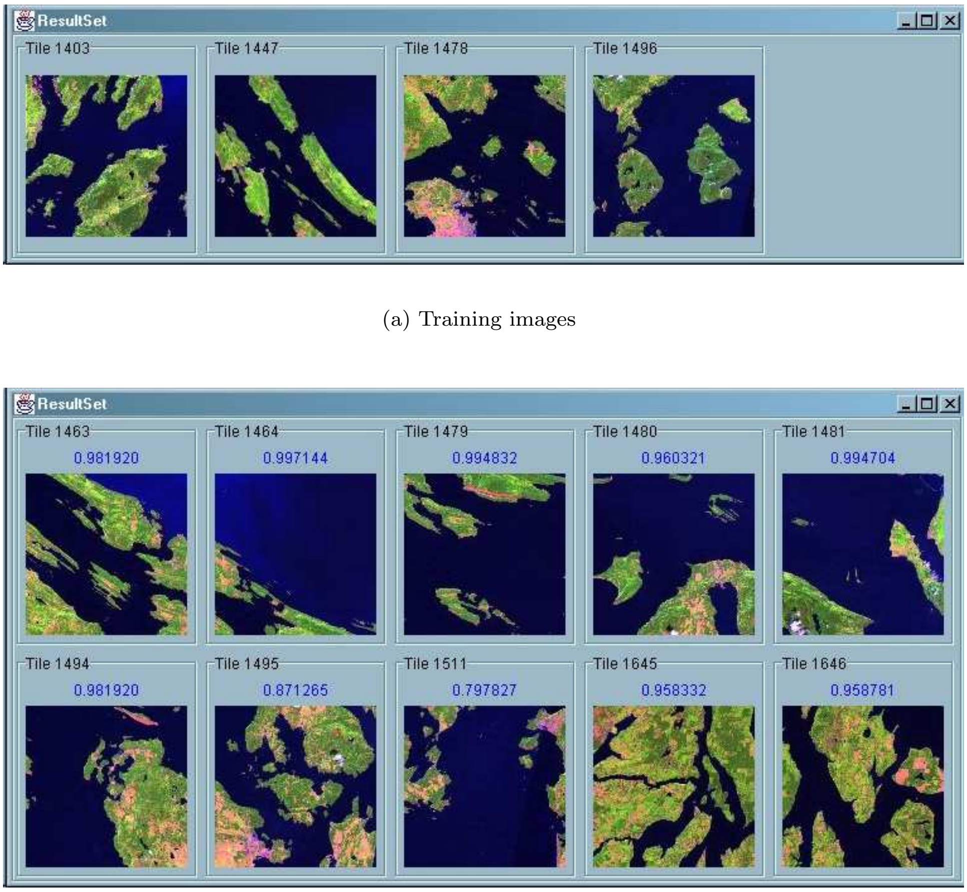

(a) Training images

(b) Images classified as containing tree covered islands

Fig. 15. Classification results for the "tree covered islands" class which is automatically modeled by the distinguishing relationships of green regions (lands covered with conifer and deciduous trees) surrounded by blue regions (water).

based on automatic selection of distinguishing (e.g. frequently occurring, rarely occurring) relations between regions.

The visual grammar overcomes the limitations of traditional region or scene level image analysis algorithms which assume that the regions or scenes consist of uniform pixel feature distributions. Furthermore, it can distinguish different interpretations of two scenes with similar regions when the regions have different spatial arrangements. We demonstrated our system with query scenarios that could not be expressed by traditional pixel, region or scene level approaches but where the visual grammar provided accurate classification and retrieval.

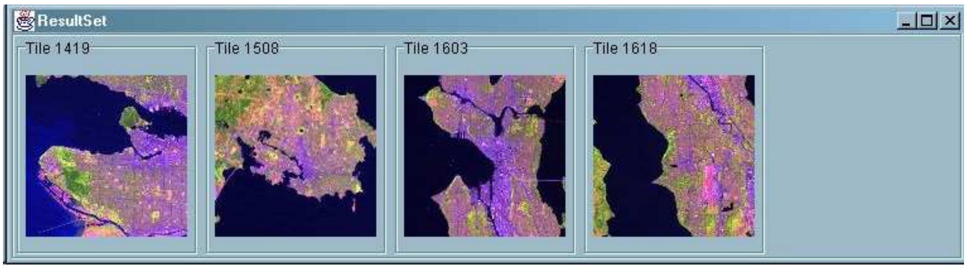

ResultSet

Tile 1419 Tile 1508 Tile 1603 Tile 1618

(a) Training images

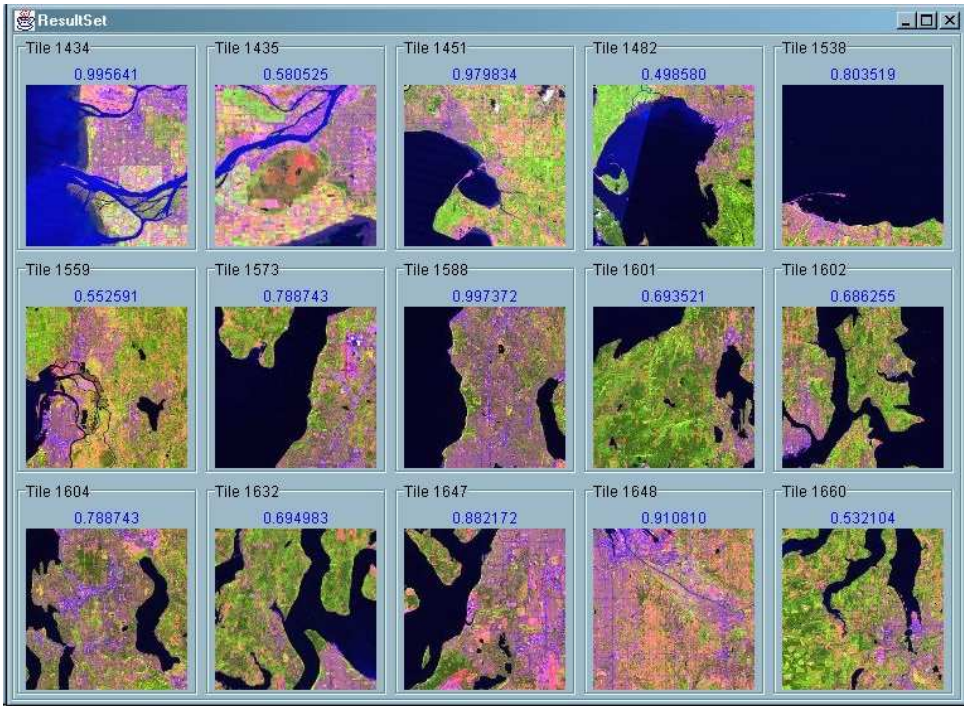

ResultSet

Tile 1434 0.995641 Tile 1435 0.580525 Tile 1451 0.979834 Tile 1482 0.498580 Tile 1538 0.803519

Tile 1559 0.552591 Tile 1573 0.788743 Tile 1588 0.997372 Tile 1601 0.693521 Tile 1602 0.686255

Tile 1604 0.788743 Tile 1632 0.694983 Tile 1647 0.882172 Tile 1648 0.910810 Tile 1660 0.532104

(b) Images classified as containing residential areas with a coastline

Fig. 16. Classification results for the "residential areas with a coastline" class which is automatically modeled by the distinguishing relationships of regions containing a mixture of concrete, grass, trees and soil (residential areas) with their neighboring blue regions (water).

Future work includes using supervised methods to learn prototype models in terms of spectral, textural and ancillary GIS features; new methods for user assistance for updating of visual grammar models; automatic generation of metadata for very large databases; and natural language search support (e.g. "Show me an image that contains a city surrounded by a forest that is close to a water source."). Insightful Corporation's InFact product is a natural language question answering platform for mining unstructured data. A VisiMine–InFact interface will be an alternative to the query-by-example paradigm by allowing natural language-based searches on large remote sensing image archives. This will especially be useful for users who do not have query examples for particular scenes they are looking for, or when transfer of large image data is not feasible over slow connections.

Acknowledgments

This work is supported by the NASA contract NAS5-01123 and NIH Phase II grant 2-R44-LM06520-02.

References

1. S. Aksoy. *A Probabilistic Similarity Framework for Content-Based Image Retrieval*. PhD thesis, University of Washington, Seattle, WA, June 2001.
2. S. Aksoy and R. M. Haralick. Using texture in image similarity and retrieval. In M. Pietikainen, editor, *Texture Analysis in Machine Vision*, volume 40 of *Series in Machine Perception and Artificial Intelligence*, pages 129–149. World Scientific, 2000.
3. S. Aksoy and R. M. Haralick. Feature normalization and likelihood-based similarity measures for image retrieval. *Pattern Recognition Letters*, 22(5):563–582, May 2001.
4. S. Aksoy, G. Marchisio, K. Koperski, and C. Tusk. Probabilistic retrieval with a visual grammar. In *Proceedings of IEEE International Geoscience and Remote Sensing Symposium*, volume 2, pages 1041–1043, Toronto, Canada, June 2002.
5. S. Berretti, A. Del Bimbo, and E. Vicario. Modelling spatial relationships between colour clusters. *Pattern Analysis & Applications*, 4(2/3):83–92, 2001.
6. G. Celeux and G. Govaert. Gaussian parsimonious clustering models. *Pattern Recognition*, 28:781–793, 1995.
7. W. W. Chu, C.-C. Hsu, A. F. Cardenas, and R. K. Taira. Knowledge-based image retrieval with spatial and temporal constructs. *IEEE Transactions on Knowledge and Data Engineering*, 10(6):872–888, November/December 1998.
8. R. O. Duda, P. E. Hart, and D. G. Stork. *Pattern Classification*. John Wiley & Sons, Inc., 2000.
9. C. Evans, R. Jones, I. Svalbe, and M. Berman. Segmenting multispectral Landsat TM images into field units. *IEEE Transactions on Geoscience and Remote Sensing*, 40(5):1054–1064, May 2002.
10. R. M. Haralick, K. Shanmugam, and I. Dinstein. Textural features for image classification. *IEEE Transactions on Systems, Man, and Cybernetics*, SMC-3(6):610–621, November 1973.
11. R. M. Haralick and L. G. Shapiro. *Computer and Robot Vision*. Addison-Wesley, 1992.
12. S. I. Hay, M. F. Myers, N. Maynard, and D. J. Rogers, editors. *Photogrammetric Engineering & Remote Sensing*, volume 68, February 2002.
13. G. G. Hazel. Object-level change detection in spectral imagery. *IEEE Transactions on Geoscience and Remote Sensing*, 39(3):553–561, March 2001.
14. G. Koepfler, C. Lopez, and J. M. Morel. A multiscale algorithm for image segmentation by variational method. *SIAM Journal of Numerical Analysis*, 31:282–299, 1994.

15. K. Koperski, J. Han, and G. B. Marchisio. Mining spatial and image data through progressive refinement methods. *European Journal of GIS and Spatial Analysis*, 9(4):425–440, 1999.
16. K. Koperski, G. Marchisio, S. Aksoy, and C. Tusk. Applications of terrain and sensor data fusion in image mining. In *Proceedings of IEEE International Geoscience and Remote Sensing Symposium*, volume 2, pages 1026–1028, Toronto, Canada, June 2002.
17. K. Koperski, G. Marchisio, S. Aksoy, and C. Tusk. VisiMine: Interactive mining in image databases. In *Proceedings of IEEE International Geoscience and Remote Sensing Symposium*, volume 3, pages 1810–1812, Toronto, Canada, June 2002.
18. K. Koperski, G. Marchisio, C. Tusk, and S. Aksoy. Interactive models for semantic labeling of satellite images. In *Proceedings of SPIE Annual Meeting*, Seattle, WA, July 2002.
19. K. Koperski and G. B. Marchisio. Multi-level indexing and GIS enhanced learning for satellite images. In *Proceedings of ACM International Workshop on Multimedia Data Mining*, pages 8–13, Boston, MA, August 2000.
20. S. Kuehn, U. Benz, and J. Hurley. Efficient flood monitoring based on RADARSAT-1 images data and information fusion with object-oriented technology. In *Proceedings of IEEE International Geoscience and Remote Sensing Symposium*, volume 5, pages 2862–2864, Toronto, Canada, June 2002.
21. K. I. Laws. Rapid texture classification. In *SPIE Image Processing for Missile Guidance*, volume 238, pages 376–380, 1980.
22. B. S. Manjunath and W. Y. Ma. Texture features for browsing and retrieval of image data. *IEEE Transactions on Pattern Analysis and Machine Intelligence*, 18(8):837–842, August 1996.
23. G. B. Marchisio and J. Cornelison. Content-based search and clustering of remote sensing imagery. In *Proceedings of IEEE International Geoscience and Remote Sensing Symposium*, volume 1, pages 290–292, Hamburg, Germany, June 1999.
24. G. B. Marchisio, K. Koperski, and M. Sannella. Querying remote sensing and GIS repositories with spatial association rules. In *Proceedings of IEEE International Geoscience and Remote Sensing Symposium*, volume 7, pages 3054–3056, Honolulu, HI, July 2000.
25. G. B. Marchisio and A. Q. Li. Intelligent system technologies for remote sensing repositories. In C. H. Chen, editor, *Information Processing for Remote Sensing*, pages 541–562. World Scientific, 1999.
26. G. B. Marchisio, W.-H. Li, M. Sannella, and J. R. Goldschneider. GeoBrowse: An integrated environment for satellite image retrieval and mining. In *Proceedings of IEEE International Geoscience and Remote Sensing Symposium*, volume 2, pages 669–673, Seattle, WA, July 1998.
27. G. J. McLachlan and T. Krishnan. *The EM Algorithm and Extensions.* John Wiley & Sons, Inc., 1997.
28. P. J. Neal, L. G. Shapiro, and C. Rosse. The digital anatomist structural abstraction: A scheme for the spatial description of anatomical entities. In *Proceedings of American Medical Informatics Association Annual Symposium*, Lake Buena Vista, FL, November 1998.
29. E. G. M. Petrakis and C. Faloutsos. Similarity searching in medical image databases. *IEEE Transactions on Knowledge and Data Engineering*, 9(3):435–447, May/June 1997.
30. J. Pickrell. Aerial war against disease. *Science News*, 161:218–220, April 6 2002.
31. J. Rissanen. Modeling by shortest data description. *Automatica*, 14:465–471, 1978.
32. A. Rydberg and G. Borgefors. Integrated method for boundary delineation of agricul-

tural fields in multispectral satellite images. *IEEE Transactions on Geoscience and Remote Sensing*, 39(11):2514–2520, November 2001.

33. S. Santini. *Exploratory Image Databases: Content-Based Retrieval.* Academic Press, 2001.
34. A. Sarkar, M. K. Biswas, B. Kartikeyan, V. Kumar, K. L. Majumder, and D. K. Pal. A MRF model-based segmentation approach to classification for multispectral imagery. *IEEE Transactions on Geoscience and Remote Sensing*, 40(5):1102–1113, May 2002.
35. M. Schroder, H. Rehrauer, K. Siedel, and M. Datcu. Interactive learning and probabilistic retrieval in remote sensing image archives. *IEEE Transactions on Geoscience and Remote Sensing*, 38(5):2288–2298, September 2000.
36. C.-R. Shyu, C. E. Brodley, A. C. Kak, and A. Kosaka. ASSERT: A physician-in-the-loop content-based retrieval system for hrct image databases. *Computer Vision and Image Understanding, Special Issue on Content-Based Access of Image and Video Libraries*, 75(1/2):111–132, July/August 1999.
37. J. R. Smith and S.-F. Chang. VisualSEEk: A fully automated content-based image query system. In *Proceedings of ACM International Conference on Multimedia*, pages 87–98, Boston, MA, November 1996.
38. L.-K. Soh and C. Tsatsoulis. Multisource data and knowledge fusion for intelligent SAR sea ice classification. In *Proceedings of IEEE International Geoscience and Remote Sensing Symposium*, volume 1, pages 68–70, 1999.
39. L. H. Tang, R. Hanka, H. H. S. Ip, and R. Lam. Extraction of semantic features of histological images for content-based retrieval of images. In *Proceedings of SPIE Medical Imaging*, volume 3662, pages 360–368, San Diego, CA, February 1999.
40. L. H. Tang, R. Hanka, H. H. S. Ip, and R. Lam. Semantic query processing and annotation generation for content-based retrieval of histological images. In *Proceedings of SPIE Medical Imaging*, San Diego, CA, February 2000.
41. J. C. Tilton, G. Marchisio, and M. Datcu. Image information mining utilizing hierarchical segmentation. In *Proceedings of IEEE International Geoscience and Remote Sensing Symposium*, volume 2, pages 1029–1031, Toronto, Canada, June 2002.
42. J. Xuan and T. Adali. Task-specific segmentation of remote sensing images. In *Proceedings of IEEE International Geoscience and Remote Sensing Symposium*, volume 1, pages 700–702, Lincoln, NE, May 1996.